J Electroceram (2011) 27:215–221
DOI 10.1007/s10832-011-9669-0

# Magnetic interactions and spin-reversal mechanism in $ErMn_{1-x}Co_xO_{3-\delta}$ samples

**C. Morilla-Santos · L. B. Arruda · C. A. Silva · P. N. Lisboa-Filho**

Received: 11 February 2011 / Accepted: 16 November 2011 / Published online: 27 November 2011


**Abstract** Manganese-based oxides present a very complex magnetic phase diagram, and many of their basic physical properties and magnetic interaction need more exploration. At the crystallographic level, the magnetic properties of rare-earth oxide manganites are strongly affected by changes in the rare-earth ion present in the structure, the nature of the transition metals, and the possibility of electronic valence fluctuations. This work studied the synthesis procedure and structural and magnetic characterization of high-quality polycrystalline samples of the $ErMn_{1-x}Co_xO_{3-\delta}$ family. Crystallographic analyses show a decrease in lattice parameters as cobalt substitution increases, accompanied by a reduction in the interatomic distances and a small increase in MT-O-MT angles (MT= cobalt and manganese) considering the c-axis. Magnetic measurements indicated a phase separation picture, and show the coexistence of different magnetic interactions with the samples considering the Mn/Co ratio. In addition, the spin-inversion mechanism is interpreted as having a crucial role in the family's magnetic response.

**Keywords** Sol–gel processes · Magnetic properties · Perovskites · Transition metal oxides

C. Morilla-Santos · L. B. Arruda · C. A. Silva
UNESP—Univ Estadual Paulista, Programa de Pós-Graduação em Ciência e Tecnologia de Materiais,
Bauru, Brazil

P. N. Lisboa-Filho (✉)
UNESP—Univ Estadual Paulista, Faculdade de Ciências,
Departamento de Física,
Bauru, Brazil
e-mail: plisboa@fc.unesp.br

## 1 Introduction

Transition metal oxide materials are strongly correlated to electronic systems in which spin, charge, lattice, and/or orbital interaction are simultaneously present. This attribute is responsible for the occurrence of many interesting physical effects such as colossal magnetoresistance (CMR), charge ordering (CO), and high temperature superconductivity (HTSC) [1].

In particular, manganites represent a unique class of strongly correlated materials due to three remarkable characteristics. In the absence of an applied magnetic field, manganites are insulators, but small magnetic fields induce metal insulator transitions. In addition, manganites present a very rich magnetic phase diagram, including competitive and cooperative phenomena. Finally, manganites present a tendency to an intrinsic inhomogeneous state at the nanoscale [2]. In fact, these three special features are all interconnected, and although the basic physical phenomena have been known since the fifties, several questions still remain in the literature, and alternative scenarios are needed to better explain the materials' magnetic response [3].

Since the perovskite structure has an $ABO_3$ formula, substitutions in the A-site may tune antiferromagnetic to ferromagnetic inducing an electronic phase separation in macroscopic regions through the sample [4]. The same behavior was observed for B-site substituted materials, where manganese ions were partly replaced with cobalt [5].

Furthermore, control of the synthesis condition and subsequent processing are responsible for defects and inhomogeneities that modify the magnetic behavior of these materials [6]. Concerning the phenomenon of phase separation, the size and shape of the particles are especially relevant since if the particle size is smaller than a single domain size, the spins are highly affected by thermal

fluctuations and ferromagnetism is replaced by superparamagnetic behavior [7].

Many contributions reported in the literature concerning the magnetic properties of manganites use synthesis procedures based on the conventional ceramic method for obtaining powders and/or sintered samples. These methods are not appropriate for many advanced applications, due to the formation of large particles, agglomerates, poor homogeneity, undesirable phases, irregular grain growth, lower reproducibility, and an imprecise stoichiometric control of cations. Otherwise, in order to enhance the powder characteristics, polymeric precursors based-routes have been used successfully to produce high-quality specimens. One of the most promising routes in chemical synthesis is based on polyesters obtained from citrates. This method, developed by Maggio Pechini and later modified [8, 9], involves two basic chemical reactions. The first is the chelation between the complex cations and the citric acid, whereas the second reaction is the polyesterification between a hydrocarboxylic acid and ethylene glycol, resulting in an acid solution.

$ErMnO_3$ is a hexagonal rare-earth manganite recently studied as a multiferroic compound [10]. This compound has competing magnetic inter and intra sub-lattice interactions formed by $Mn^{3+}$ (3 d $^4$) and $Er^{3+}$ (4f $^{11}$) ions, forming a geometrically frustrated structure where ordering of the $Er^{3+}$ spins at low temperature is expected, and a weak magnetic transition close to 75 K is associated with an antiferromagnetic ordering temperature of Mn ions [11, 12].

The system $ErMn_{1-x}MT_xO_{3-\delta}$, where MT is a divalent transition metal has been studied as a prototype material to better understand the substitutions at the manganese sites, since $Mn^{3+}$ is transformed into $Mn^{4+}$, induced by a charge transfer effect due to hole doping [13]. In this system, the manganese atom can be substituted with cobalt in orthorhombic symmetry with the space group Pbnm [14].

## 2 Experimental details

The samples were synthesized using the polymeric precursor method, starting from metallic ions dissolving in aqueous solution and using citric acid ($C_6H_8O_7$) as the chelating agent, following the flowchart shown in Fig. 1.

Initially, stoichiometric amounts of $Er_2O_3$, $MnCO_3$ and $Co(NO_3)_2.6H_2O$ were dissolved into desionized water by adding $HNO_3$. These dissolved salts were mixed with citric acid solution at a metal/chelating agent proportion of 1:3. After 1 h at 60°C, the solution was polymerized by adding ethylene glycol at a citric acid/ethylene glycol mass ratio of 60:40 [15]. The chelation and polymerization reactions are outlined in Fig. 2. Under constant stirring, ethylenediamine was added until the pH of the solution was 5. The temperature was increased to 90°C in order to evaporate the water and form the gel. Then the gel was pyrolyzed at 350°C/2 h, resulting in amorphous powder that was then heat treated in steps of 700°C, 900°C, and 1000°C ($O_2$ flux) for 8 h each to obtain the crystalline phase. Four sets of samples were prepared and were labeled $ErMnO_3$ (EMO), $ErMn_{0.60}Co_{0.40}O_{3-\delta}$ (Mn60), $ErMn_{0.50}Co_{0.50}O_{3-\delta}$ (Mn50), and $ErMn_{0.40}Co_{0.60}O_{3-\delta}$ (Mn40).

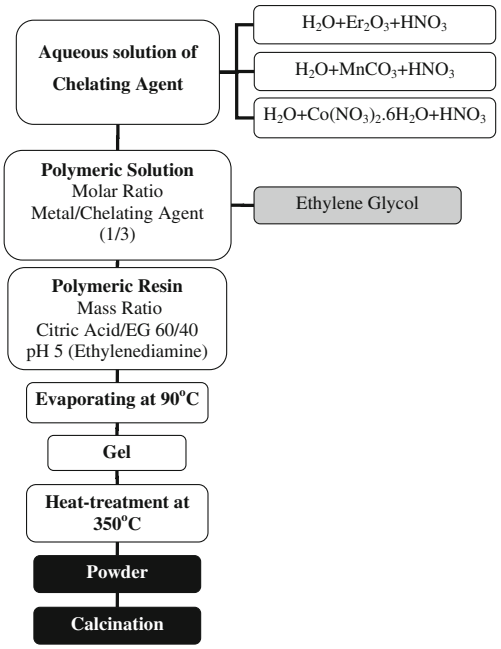


**Fig. 1** Flowchart of the $ErMn_{1-x}Co_xO_{3-\delta}$ sample preparation by the modified polymeric precursors method

Crystallographic phases were analyzed with X-ray diffraction in a Rigaku DMAX 2100/PC diffractometer, and structural analyses were performed using Rietveld refinement under GSAS software [16]. The magnetic measurements were performed with a Quantum Design MPMS XL-5 SQUID Magnetometer. Measurements of magnetization as a function of temperature were taken in ZFC (zero field cooling) and FC (field cooling) procedures. Moreover, magnetization vs. the magnetic applied field was also carried out.

## 3 Results and discussion

Oxygen content, and consequently manganese and cobalt valences highly influence the magnetic response for the samples. Redox titration techniques were used to determine manganese valence fluctuations, and by charge-equilibrium arguments the oxygen content of the samples can be estimated. The average obtained result indicated that the oxygen stoichiometry for the sample as it was prepared was $3-\delta=2.90$ ($\pm0.05$) [15].

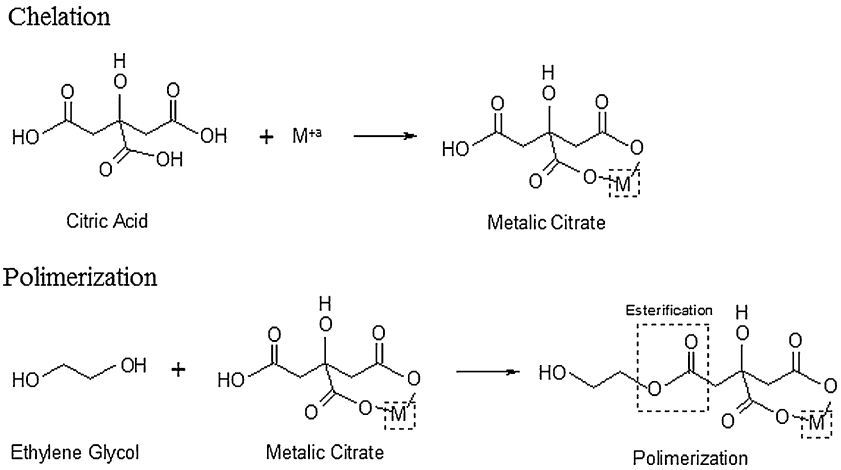


**Fig. 2** Chemical reactions in the polymeric precursors method

X-ray diffraction analyses associated with Rietveld refinement confirm that the synthesized erbium manganese oxide sample ($ErMnO_3$) is single phase with hexagonal symmetry and a $P6_3cm$ space group. Otherwise, the cobalt substitute samples present orthorhombic symmetry with the Pbmn space group. Details of symmetry, lattice parameters, volume, and refinement statistics are presented in Table 1. The obtained results indicated the quality of the prepared samples with parameters very close to those observed in high-quality single crystals [17]. In addition, a small amount (3.1%) of $Er_2O_3$ was detected for the Mn40 sample.

The data presented in Table 1 show, for samples of orthorhombic symmetry, that the increase in cobalt content is accompanied by a reduction in unit cell volume. For the $ErMn_{1-x}Co_xO_{3-\delta}$ family, the literature reports that substitutions with ions $Co^{2+}$ are limited to 50% due to the charge balance. However, higher substitutions may occur since both oxidation states $Co^{2+}$ and $Co^{3+}$ are possible [18]. The literature also reports that heat treatments in the atmosphere of $O_2$ favor the presence of $Co^{3+}$, which is crucial, since the magnetic properties are related to the presence of different ions ($Er^{3+}$, $Co^{2+}$, $Co^{3+}$, $Mn^{3+}$, $Mn^{4+}$) [19]. Thus, the reduction in volume of the unit cell can be explained in terms of the possibility of the valence state of cobalt. Initially, $Mn^{+3}$ was replaced with $Co^{2+}$ to the limit of the charge balance. For higher contents of cobalt associated with the heat treatment atmosphere of $O_2$, and considering the charge balance, $Mn^{+4}$ being replaced by the $Co^{3+}$ ion, the smaller ionic radius caused a reduction in the unit cell volume [19].

Figure 3 shows the Rietveld refinements for the $ErMn_{0.5}Co_{0.5}O_{3-\delta}$ sample, and two profiles of the refined

**Table 1** Structure and crystallographic results of the Rietveld refinement

| | | | Symmetry | Space group |
|---|---|---|---|---|
| Molecular formula | : $ErMnO_3$ (EMO) | | Hexagonal | $P6_3cm$ |
| | : $ErMn_{0.60}Co_{0.40}O_{3-\delta}$ (Mn60) | | Orthorhombic | Pbnm |
| | : $ErMn_{0.50}Co_{0.50}O_{3-\delta}$ (Mn50) | | Orthorhombic | Pbnm |
| | : $ErMn_{0.40}Co_{0.60}O_{3-\delta}$ (Mn40) | | Orthorhombic | Pbnm |
| Chemical synthesis | : Pechini method | | | |
| Unit cell-parameters | a (Å) | b (Å) | c (Å) | V (Å$^3$) |
| EMO | 6.116(9) | 6.116(9) | 11.398(7) | 369.36(1) |
| Mn60 | 5.220(3) | 5.600(2) | 7.459(1) | 218.06(1) |
| Mn50 | 5.212(3) | 5.573(4) | 7.454(5) | 216.56(3) |
| Mn40 | 5.190(9) | 5.539(1) | 7.434(2) | 213.75(4) |

$\chi^2$: EMO=2.23, Mn60=1.26, Mn50=1.10, Mn40=1.89

$R_{Bragg}$: EMO=5.89%, Mn60=4.54%, Mn50=4.17%, Mn40=4.41%

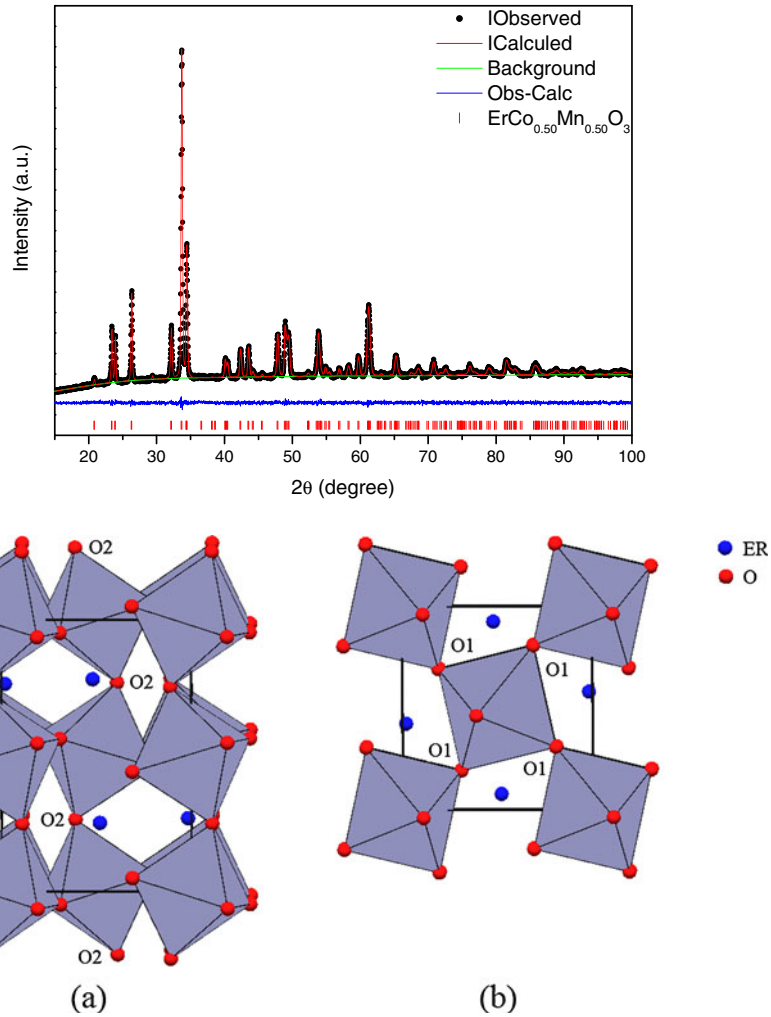


**Fig. 3** (**a**) Rietveld refinements for the $ErMn_{0.5}Co_{0.5}O_{3-\delta}$ sample. (**b**) Refined unit cell of $ErMn_{1-x}Co_xO_{3-\delta}$

unit cell of the $ErMn_{1-x}Co_xO_{3-\delta}$ family are shown in Fig. 3(a) and (b). The erbium atoms are in blue and the oxygen atoms in red. In addition, Fig. 3(a) and (b) show the polyhedra around manganese or cobalt atoms, linked to oxygen, and demonstrating the degree of distortion of the structure in relation to an ideal cubic perovskite. Table 2 presents the values of some interatomic distances and angles.

**Table 2** Angles and distances interatomics

| Angles (°) | Distances (Å) |
|---|---|
| $ErMn_{0.60}Co_{0.40}O_{3-\delta}$ | |
| MT-O1-MT : 145.002(5) | MT-O1 : 2.031(5) |
| MT-O2-MT : 143.753(3) | MT-O2 : 1.962(1) |
| $ErMn_{0.50}Co_{0.50}O_{3-\delta}$ | |
| MT-O1-MT : 144.959(1) | MT-O1 : 2.023(2) |
| MT-O2-MT : 143.796(4) | MT-O2 : 1.960(7) |
| $ErMn_{0.40}Co_{0.60}O_{3-\delta}$ | |
| MT-O1-MT : 144.919(2) | MT-O1 : 2.011(2) |
| MT-O2-MT : 143.851(2) | MT-O2 : 1.955(1) |

The mean distances of transition elements to oxygen decrease as the cobalt content increases, a result consistent with the explanation in the preceding paragraph. The table

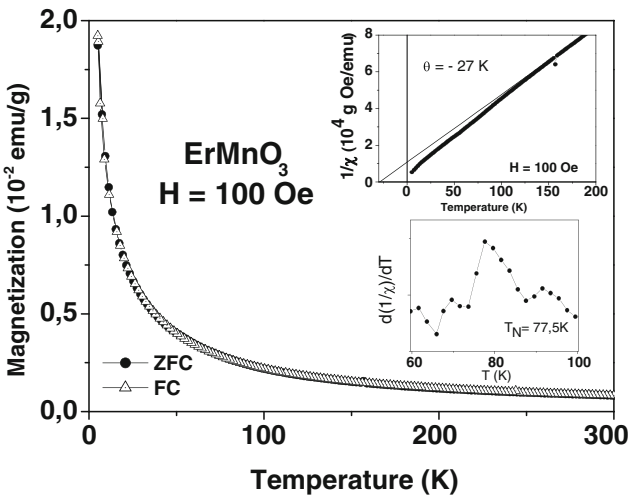


**Fig. 4** Magnetic response $ErMnO_3$ sample. In the inset is shown the reciprocal magnetic susceptibility

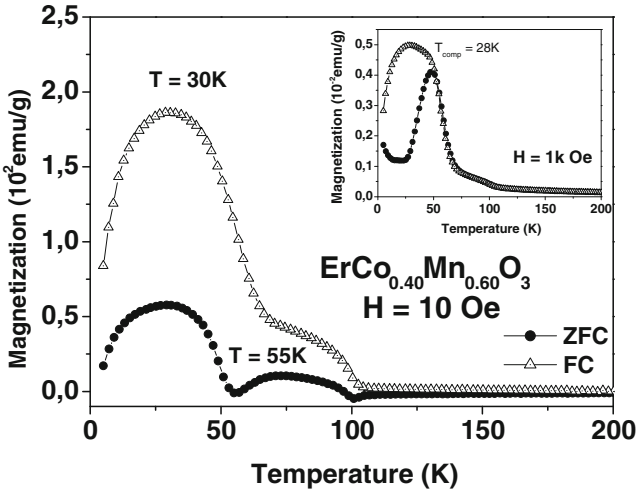


**Fig. 5** Magnetic response of the $ErCo_{0.40}Mn_{0.60}O_{3-\delta}$ sample

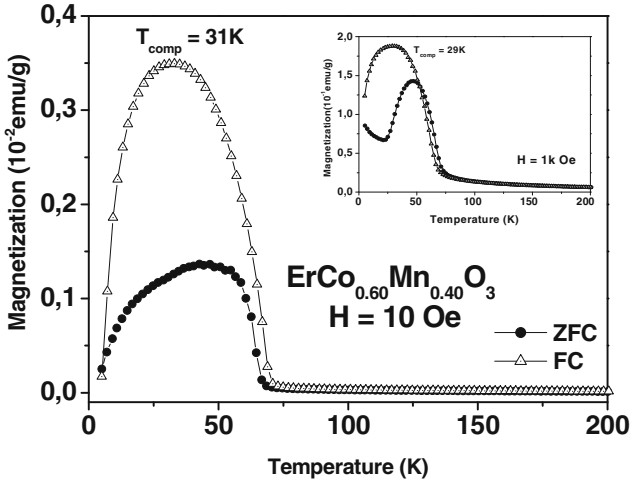


**Fig. 7** Magnetic response of the $ErCo_{0.60}Mn_{0.40}O_{3-\delta}$ sample

also shows the reduction in the MT-O1-MT angle and the increase in the MT-O2-MT angle. These results show a small increase in the distortion of polyhedra considering O1 atoms, and a reduction in the polyhedra along the c-axis.

The magnetic response of the $ErMnO_3$ sample follows the Curie-Weiss law with θ of −27 K, as shown in Fig. 4. In addition, in the inset of Fig. 4 the derivative of the reciprocal of magnetic susceptibility can be observed, which indicates an antiferromagnetic ordering transition of Mn ions close to 77 K, in accordance with previous reports [6, 20].

Magnetization as a function of temperature curves under ZFC (zero field cooled) and FC (field cooled) cycles for the $ErMn_{1-x}Co_xO_{3-\delta}$ samples can be observed in Figs. 5, 6 and 7, and reveals the competition and interaction of Co-Mn. In addition, for the Er sub-lattices, the first is aligned to the external applied magnetic field and the later negatively aligned to the external field.

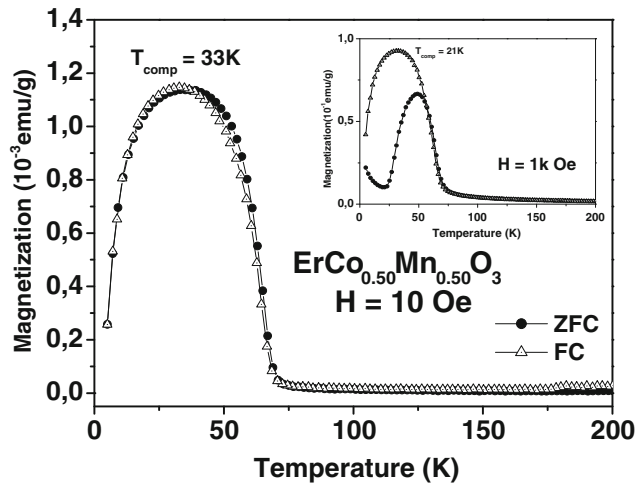


**Fig. 6** Magnetic response of the $ErCo_{0.50}Mn_{0.50}O_{3-\delta}$ sample

The effects of Co ionic substitutions in manganite compounds have been studied in the literature, and are still a controversial issue [21, 22]. Starting from antiferromagnetic phases, it seems that cobalt substitutions in manganese sites induce ferromagnetism in a phase separation scenario, with two different types of superexchange interactions. Joly and co-workers reported for $LaMn_{1-x}Co_xO_3$ samples that the coexistence of magnetic phases are dependent of processing temperature for x>0.5, and mixed-phase behavior occurs for samples with $x$=0.5 [23]. They also argued that the magnetic transition temperatures are independent of Co composition, as an indication of phase separation.

Thermal irreversibility in this system is explained assuming that during the ZFC curve the magnetic sub-lattices are uncoupled and experience the same external field. Consequently, the canted antiferromagnetism of the |Mn+Me| network and the Curie–Weiss behavior of the Er sub-lattice will contribute independently to the total magnetization.

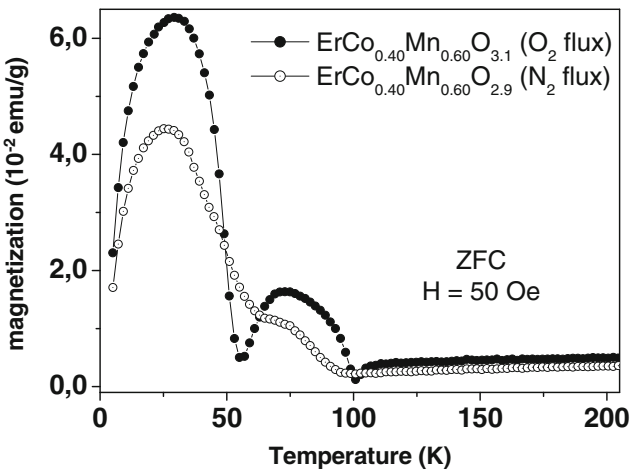


**Fig. 8** ZFC run for the $ErCo_{0.40}Mn_{0.60}O_{3-\delta}$ sample annealed in gas flux at 550°C for 6 h

Otherwise, during the FC run, the transition-metal sub-lattice will order at an ordering temperature, provoking a local field to the erbium moments. The resulting magnetization will be the superposition of the magnetic response of both sub-lattices.

For all samples, the ZFC runs presented the usual antiferromagnetic spin-canted behavior, with inter-plane antiferromagnetic interactions and intra-plane ferromagnetic interactions. When the applied magnetic field is increased (inset of Figs. 5, 6 and 7), the magnetic ordering temperature $T_C$ is clearly seen around 70 K, and no cobalt content dependence on $T_C$ is observed, as already observed for samples synthesized by solid state reaction routes [13]. Interestingly for the Mn60 sample (Fig. 5) measured at lower magnetic field, two remarkable responses are present. The first one is an enhancement on magnetic transition if compared to solid state prepared samples, possibly associated to particle size effects [9]. It also can be seen that two maxima are detected in the ZFC run, the one at lower temperatures associated an ordering due to Er sublattices and another related to the intrinsic behavior of the Mn+Co network [19]. At lower fields in the ZFC run the minimum of temperature at 55 K may represent the compensation point of these two configurations.

The independence of the transition temperatures for higher substitution samples (Figs. 6 and 7) is evidence that phase separation plays a major role in the magnetic response of these samples. Otherwise, during the FC runs, an interesting behavior is also observed where the total magnetic moment of the sample, formed by Er moments and Mn-Co moments, reverses opposite to the applied magnetic field in the compensation temperature ($T_{comp}$) [19]. This response can be interpreted by the fact that during the FC run, Co-Mn moments order ferromagnetically producing an internal field at the Er site, ordering and enhancing the contribution of erbium moments. Considering a negative interaction between Er- and Mn-Co moments when at lower temperatures the contribution of erbium to the total moment increases, the total magnetic moment of the sample flips, opposing the applied field at $T_{comp}$. Considering the analyses of the FC runs, although cobalt substitution induces ferromagnetism as previously reported, it is clear that for cobalt-substituted $ErMnO_3$ samples the spin-inversion mechanism prevails.

Another distinctive feature of the observed magnetic response is that some of the magnetic transitions' temperature and behavior are more diverse than observed in samples prepared by solid state reaction routes [15, 18]. A plausible explanation for that must take into account particle size effects and oxygen content in Sol–gel derivate samples, which are highly different from solid state route-based samples. In order to test oxygen stoichiometry effects, some Mn60 samples were annealed for 6 h at 550°C in gas flux (oxygen or nitrogen), and the magnetic response of the samples can be seen in Fig. 8. The oxygen content was also estimated for these samples for $Mn60/O_2$ as $3-\delta=3.00$ ($\pm0.05$) and $Mn60/N_2$ as $3-\delta=2.80$ ($\pm0.05$). A different feature in the second maximum was detected for the sample heat-treated in $N_2$ flux, indicating that response can be associated with $Co^{2+}$ ions since oxygen-flux heat-treatment induces the increase of $Co^{3+}$ specimens in the sample. Moreover, an increase in the temperature maximum at lower temperatures and an enhancement of the spin inversion mechanism at $T_{comp}$ are also observed, indicating that Mn-$Co^{+3}$ moments are responsible for that response.

## 4 Conclusions

Polycrystalline samples of $ErMn_{1-x}Co_xO_{3-\delta}$ family were prepared by a modified polymeric precursor route, and the obtained structural data are comparable to single crystal lattice parameters.

Cobalt substitute manganites present a phase separation scenario characterized by an increase of the ferromagnetism as a function of cobalt doping. However, for the $ErMn_{1-x}Co_xO_{3-\delta}$ system the prevalence of spin-inversion was observed at low temperatures. This response is associated with competitive and cooperative phenomena between ferromagnetic $Mn^{3+}$ - $Mn^{4+}$ ions and antiferromagnetic exchange interactions in the Er-MT sub-lattices. As this family presents $Er^{3+}$, $Mn^{3+}$, $Mn^{4+}$, $Co^{3+}$, and $Co^{+2}$ ions, a complex and rich magnetic response is observed, and annealing at different gas fluxes induced some modifications in the magnetic behavior. In addition, distinctive magnetic responses observed in this contribution are not observed in samples prepared by solid state routes.

**Acknowledgements** The authors wish to thank the Brazilian agencies Fundação de Amparo à Pesquisa do Estado de São Paulo (FAPESP, Grant 2007/08072-0) and Conselho Nacional de Desenvolvimento Científico e Tecnológico (CNPq, Grant 303776/2007-2).

## References

1. E. Dagotto, Science **309**, 257 (2005)
2. E. Dagotto, J. Burgy, A. Moreo, Solid State Comm. **126**, 9 (2003)
3. M.B. Salamon, M. Jaime, Rev. Mod. Phys. **73**, 583 (2001)
4. M. Uehara, S. Mori, C.H. Chen, S.W. Cheong, Nature **399**, 560 (1999)
5. V.L. Joseph, P.A. Joy, S.K. Date, J. Phys. Condens. Mater **13**, L841 (2001)
6. B. Raveau, J. Eur. Ceram. Soc. **25**, 1985 (2005)
7. A. Rostamnejadi, H. Salamati, P. Kameli, H. Ahmadvand, J. Mag. Mag. Mater. **321**, 3126 (2009)
8. M. Pechini, US Patent 3330697 (1967).
9. P.N. Lisboa-Filho, A.W. Mombru, H. Pardo, W.A. Ortiz, E.R. Leite, J. Phys. Chem. Solids **64**, 583 (2003)
10. J.R. Sahu, A. Gosh, A. Sundaresan, C.N.R. Rao, Mater. Res. Bull. **44**, 2123 (2009)

11. M.C. Sekhar, S. Lee, G. Choi, C. Lee, J.G. Park, Phys. Rev. B. **72**, 14402 (2005)
12. S.Y. Jang, D. Lee, J.-H. Lee, T.W. Noh, Y. Jo, M.-H. Jung, J.-S. Chung, Appl. Phys. Lett. **93**, 162507 (2008)
13. O. Peña, A.B. Antunes, M.N. Baibich, P.N. Lisboa-Filho, V. Gil, C. Moure, J. Mag. Mag. Mater. **312**, 78 (2007)
14. C. Moure, D. Gutiérrez, O. Peña, P. Durán, J. Am. Ceram. Soc. **86**, 54 (2003)
15. P.N. Lisboa-Filho, M. Bahout, P. Barahona, C. Moure, O. Peña, J. Phys. Chem. Solids **66**, 1206 (2005)
16. A.C. Larson, R.B. Von Dreele. General Structure Analysis System (GSAS). Los Alamos National Laboratory Report LAUR 86–748 (2004).
17. A.B. Antunes, M. Ceretti, W. Paulus, T. Roisnel, V. Gil, C. Moure, O. Peña, J. Mag. Mag. Mater. **320**, 69 (2008)
18. A.B. Antunes, O. Peña, C. Moure, V. Gil, G. André, J. Mag. Mag. Mater. **316**, 652 (2007)
19. A.B. Antunes, V. Gil, C. Moure, O. Peña, J. Eur. Ceram. Soc. **27**, 3927 (2007)
20. A.P. Litvincuk, M.N. Iliev, V.N. Popov, M.M. Gospodinov, J. Phys, Condens. Matter **16**, 809 (2004)
21. P.A. Joy, Y.B. Khollam, S.K. Date, Phys. Rev. B. **62**, 8608 (2000)
22. Y. Ying, N.V. Dai, T.W. Eom, Y.P. Lee, J. Appl. Phys. 105 093924.
23. V.L. Joly, P.A. Joy, S.K. Date, J. Phys. Condens. Mater **13**, L841 (2001)